A power management system for electromagnetic energy harvesters in battery/batteryless applications

Mahmoud Shousha, Dragan Dinulovic, *Member*, *IEEE*, Martin Haug, Tomislav Petrovic, and Abdelmomen Mahgoub

Abstract— **This paper presents a miniaturized and cost effective power management system (PMS) for low-voltage electromagnetic energy harvesters (EMEHs) operating in both battery powered and batteryless applications. The PMS consists of two converters and their associated controllers. The first converter converts EMEH's ac voltage into a dc one in a single step and provides a maximum efficiency point tracking (MEPT) feature to maximize the harvested energy and can be used alone in battery powered applications. The second converter provides tight output voltage regulation for batteryless applications. The MEPT converter utilizes a topology that uses a single inductor shared between positive and negative half cycles of the EMEH voltage, unlike the majority of existing solutions, and hence achieving system's cost and size reductions. In addition, its control architecture is based on low power comparators and does not require zero crossing detection (ZCD) block, in contrast to many existing solutions, allowing for further reduction in cost, losses, and size. Moreover, the shared inductor is not only used by the power stage but also as a key element of the bias supply scheme allowing for voltage stepping up and hence providing sufficient voltage to supply the control circuits. The voltage regulation converter features a highly integrated dc-dc converter where the power inductor serves as normal inductor and a substrate for the converter.**

Experimental results show the effectiveness of the PMS with an EMEH that has a damped ac voltage characteristics ranging from 1.0V to 10mV for battery and batteryless applications. The presented MEPT converter, switching at 40KHz, achieves 32.3 mm^3 magnetics volume, which is the biggest contributor to the real estate of the PMS. Also, it can harvest up to 17mJ out of 20mJ available energy while achieving a BOM cost less than 0.7€. Moreover, the highly integrated buck converter, switching at 4MHz, provides a tight regulated voltage of 1.2V at 5mA for a group of wireless sensors while achieving efficiency of 80% for load currents between 100µA and 200mA.

Index Terms— **Energy harvesters, power management system, electromagnetics, Power electronics topologies.**

I. Introduction

Energy harvesting from ambient sources presents a potential solution to supply low power devices installed in remote areas and/or where the costs of installing and replacing batteries are prohibitively high. A partial solution for this problem is extending battery-operating time by storing the energy harvested from ambient sources. Relying fully on ambient sources to replace batteries can solve such issues as associated maintenance costs and/or the need for human intervention are eliminated. An example of an application that can benefit from extending the battery operating time is integrating an energy harvesting device in the shoes of athletes. It would harvest energy during running or jogging and storing the harvested energy in the battery used with wearable devices such as smart watches to extend their operating time [1]-[3]. An example of a medical application would be leg transplants where a pressure sensor measures the pressure applied to the transplanted limb continuously and provides a warning or indication in case the user exceeds the rated specifications. A battery that needs to be active all the time when the user is moving powers this sensor. In case the battery discharges completely while the user is still moving, the transplanted limb could be damaged. Harvesting energy when the transplanted limb hits the ground and storing this energy in the battery of the pressure sensor can be a solution for such a problem. A third application is extending the operating time of the batteries of electronic locking systems [4]-[5] where an energy harvesting device within the door translates the door's movement into energy used to extend the operating time of the batteries that power the lock system. As a result, a significant reduction in maintenance cost associated with replacing depleted batteries can be achieved [5], especially in facilities which rely heavily on electronic door lock systems such as hotels and universities. A large set of applications that can use energy harvesters as replacement for batteries exist in the internet of things (IoT). IoT represents the future of the world, as it will change the way companies, cities, governments, and consumers connect and interface with the world. The IoT consists of sensors and a multitude of smart objects that identify and gather surrounding data and communicate them throughout the day. A typical application in an IoT system is to install an energy harvester in the backside of a window so that when the window is closed and then opened

M. Shousha, D. Dinulovic, and M. Haug are with Magi^{3}C Division, Würth Elektronik eiSos, Munich Office, 85748 Garching, Germany. T. Petroivc is with Faculty of Mechanical Engineering, University of Niš, 18000 Niš, Serbia.

A. Mahgoub and M. Shousha are with Electrical Power Engineering Department, Cairo University, 12611 Giza, Egypt.

the energy harvester can supply sensors that transmit data, such as humidity and temperature, to the base station [6]. It is expected that there will be 55 billion connected IoT devices by 2025 all over the world and that around 15 trillion dollars will be spent on IoT devices by 2025 [7]. The main bottleneck for IoT is the high cost of integration and powering of such devices [6]. Energy harvesting is the most promising solution to cut these costs by providing a sustainable power source for such devices. However, energy harvesters (EHs) still suffer from low available energy levels, which limit their utilization to a specific range of applications. It should be noted that the term energy, not power, is used throughout the entire paper since the operation of energy harvesters is tied, in most of the cases, to a certain event that creates a certain power for a certain amount of time.

The application targeted by the work presented in this paper is harvesting the mechanical energy of a moving window and rectifying the electrical energy generated using a PMS. It is worth mentioning that higher power loads require both an energy harvester and a battery while lower power loads can be sufficiently supplied by an energy harvester alone. That means the developed PMS should have the capability to work with both battery powered and batteryless applications. Two important requirements for the application are the cost and the efficiency of the PMS since the motivation for the application is to effectively replace batteries and their surrounding costs [8]. An important secondary design goal for this work is to have the PMS usable in a wide range of energy harvesting applications beyond those discussed in this paper, therefore the overall size of the PMS is taken into consideration.

The application targeted by the work within this paper requires an energy harvesting device that translates mechanical energy into electrical energy. The most commonly used energy harvesting devices that can achieve this criterion are electromagnetic energy harvesters (EMEHs) [9]-[13] and piezoelectric generators [14]-[16]. Both types produce ac voltage and require maximum efficiency point tracking (MEPT). Piezoelectric generators have the advantage of higher output voltages [14], up to a few volts, which relaxes the requirements of the required PMS. On the other hand, they produce relatively low output power [14]-[16]. EMEHs have the opposite characteristics, with higher output energy [10] and lower output voltage, with ranges from a few mVs to hundreds of mVs [9]-[11]. The availability of higher energy, in terms of the extracted power from a specific event, in EMEHs makes it more appealing for the targeted applications. The requirements for the PMS that can be effectively used with EMEH in the previously mentioned systems is that the topology is able to convert from ac to dc voltages, and at the same time providing MEPT feature [17]-[21] to maximize harvested energy. That means the topology can be tuned to operate at the point where the energy harvester produces its maximum energy and has its highest efficiency. The conventional solution of using diode bridge rectifiers [12], [13], [17], [20]-[22] cannot be used with EMEHs due to the threshold voltage drop of the diodes. In addition, use of a synchronous bridge rectifier at the input is not ideal [20] as it increases systems complexity associated with gate driving as well as to avoid the lack of MEPT inherent in synchronous bridge rectifiers. An alternative is to use active diode rectifiers [23]-[24] where MOSFETs turn on and off by a comparator referencing their drain and source voltages. However, this solution requires an additional voltage source to supply the comparator, which is hard to achieve in many applications where energy harvesting is required. Solutions based on voltage multipliers such as Villard and Dickson charge pumps [25]-[27] can be used to multiply the input voltage of the EMEH, however, these solutions cannot implement the MEPT feature to the EMEH. Dual phase bridgeless solutions [28]-[31] get rid of the diodes, however, they are relatively bulky, relying on two inductors to achieve ac-dc conversion. Another problem with this class of converters is their gate driving requirements that usually involve having a high side gate driver. High side gate drivers and bias supply scheme are difficult to implement with low voltage harvesters, rarely appearing in literature, and typically requiring additional external supplies [30]-[31]. Another approach based on using a transformer to step up the voltage with an MEPT/ac-dc converter is shown in [32]-[34]. The main disadvantage of this approach is the increase in solution size and weight due to the transformer, in addition to complex gate driving. The authors of [35] proposed an MEPT-capable topology that converts an ac voltage into a dc one using a single inductor. However, to drive the top side MOSFET successfully, the converter must operate with energy harvesters that have voltages lower than 0.5V, a constraint the will render it unusable with many existing energy harvesting mechanisms. Additionally, the arrangement of the switches in the converter requires a ZCD circuit, comprising of a reference voltage and an operational amplifier, increasing system cost, losses, and size. An external supply is also needed to power the digital controller, further distancing the solution from the requirements of the energy harvesting applications. The authors of [36] also presented a MEPT converter using a single inductor but requiring two external power sources to start the converter. This limits the advantages obtained by such a system since the external sources are battery based and require replacement and maintenance.

The primary objective of this paper is to introduce the PMS, shown in Fig.1, for EMEHs. The PMS provides an MEPT feature and tight output voltage regulation, for battery powered or batteryless applications, while achieving improvements in size, efficiency, and cost. In addition, the PMS utilizes a simple control circuit and a gate drive cutting the main component requirements compared to other solutions such as ZCD block.

II. The Developed Electromagnetic Energy Harvesters

The presented harvester converts the mechanical energy into electrical energy using the principles of electromagnetism. The harvester is driven by pushing a button and the linear movement of the button is converted into rotation. The energy harvester system consists of (i) a mechanism for movement conversion, (ii) an electromagnetic energy harvesting transducer, and (iii) a power management system (PMS). As mentioned earlier, the motion of the driving button is linear translation; therefore, a

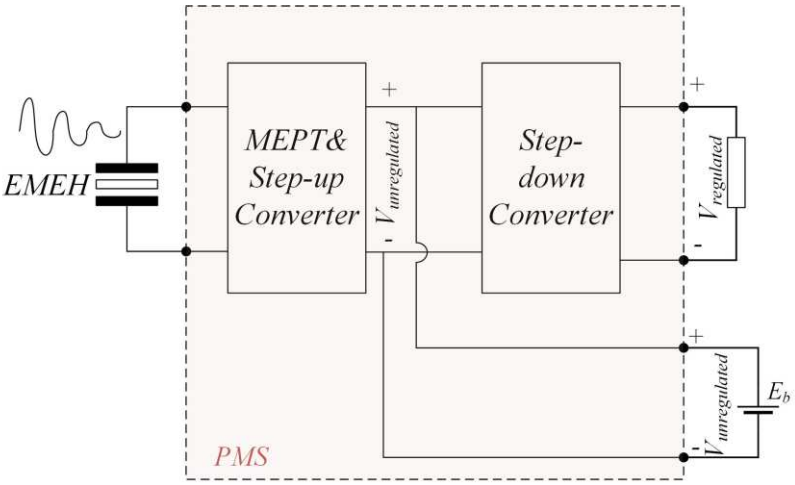

Fig. 1: Block diagram of the presented PMS.

system for motion conversion should be integrated in the harvester. Using a movement-conversion mechanism, the small linear motion of the button of about 10mm - 15mm is converted into rotation with speeds higher than 1000rpm [37].

The conversion mechanism consists of a button, round gear rack, spring, and gear with a one-way clutch. For this harvester ype, it is important to generate rotation only in one direction as allowing rotation in the opposite direction will reduce the kinetic energy transferred to the coil, resulting in a reduction of the total energy harvested. Therefore, the one-way clutch is applied to limit the rotation to one direction. The gear with a one-way clutch is a standard mechanical part and the round gear rack is easy to fabricate by traditional machining techniques. The use of standard and easy-to-fabricate parts helps to reduce the total cost of the energy harvester. Figure 2 shows the first prototype of the fabricated EH device with its main components. By pressing the button, the spring is loaded and the energy is stored in the spring. During release of the spring, the button and round gear rack move back to the starting position.

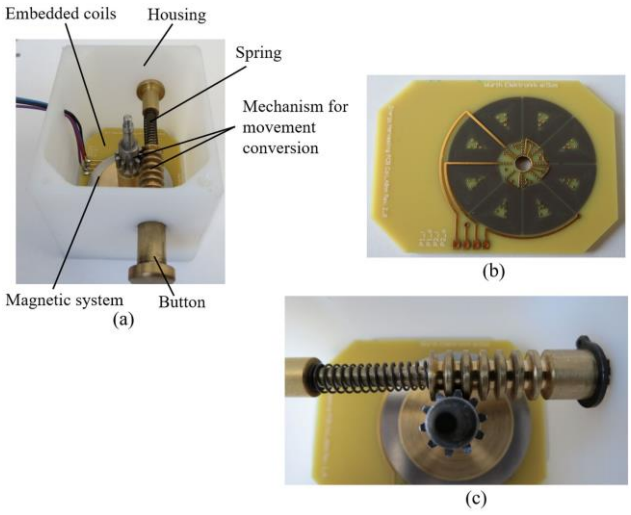

Fig. 2: (a) Components of the electromagnetic energy harvester, (b) Embedded coils in PCB, (c) The rotor.

The round gear rack moves the gear while the one–way clutch allows free rotation of the rotor with assembled permanent magnets. The rotational speed reached values of about 1000rpm.

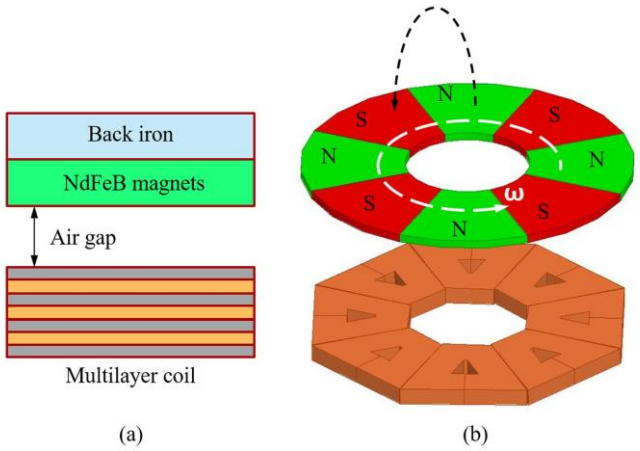

Fig. 3: (a) Structure of the generator. (b) 3-D schematic of the electromagnetic generator.

The electromagnetic part of the harvester adopts the same configuration of a standard axial flux machine. The electromagnetic part consists of a rotating portion (rotor) and stationary portion (stator). The rotor has 8-multi pole NdFeB permanent magnet segments mounted on a soft magnetic plate (back iron) with a high saturation flux density. The permanent magnet material used is BMN-44H produced by Bomatec. These permanent magnets feature a magnetic remanence, B_r, of 1.35 T and a nominal maximum energy product (BH_{max}) of 334 kJ/m³. The Co-alloy based soft magnetic plate used is aVacoflux48 material produced by Vakuumschmelze. Vacoflux48 shows very high saturation flux density, B_S, of 2.35 T. A magnetic material with high saturation flux density is necessary to avoid magnetic saturation of the system. The stator consists of 8 coils grouped into a single phase. A PCB coil embedded into FR4-ceramic material is adopted to reduce the thickness of the stator. Both the stator and the rotor are mounted

on the same axis axis forming a defined 1 mm air gap between the two portions. The outer radius of coil, $R_{o,}$ is 20 mm, the inner radius is, $R_{i,}$ is 8 mm, and the height of the coil is 12 mm. Each coil consists of 10 layers with 7 turns per layer. The turn width is 400 µm with a thickness of 105 µm. Figure 3 shows the schematics of the electromagnetic part of the harvester.

A) Analytical Estimation

The energy harvesting generator is basically a planar axial flux machine without complicated structures like poles and teeth. The magnetic flux flows from one hard magnet pole through the coil to the next magnet pole. The analytical description of similar kind of generators is shown in some research works [38]–[40]. According to [38], a simplified equation (1) can be used to calculate analytically the generated voltage linked to design parameters. As given by the equation, the single-phase open-circuit voltage, V_{oc}, is proportional to system size (inner R_i and outer R_o coil radius), thickness, t_{PM}, of the permanent magnet, thickness, t_{AG}, of the air gap, thickness of the coil system, t_{Coil}, remanence, B_r, of the permanent magnet, the number of poles, P, the number of turns per pole, N, and the angular velocity, Ω_R.

$$V_{oc} = k(R_o^2 - R_i^2).\left(\frac{t_{PM}}{t_{PM}+t_{Coil}+t_{AG}} B_r\right) NP\Omega_R, \quad (1)$$

where k is a constant that depends on the winding distribution of the stator. The maximum output power of the permanent magnet based energy harvesting generator can be calculated from maximum power transfer theory as follows:

$$P_{mout} = \frac{V_{oc}^2}{4R_{coil}}, \quad (2)$$

where R_{coil} is the total resistance of the coils. For a system with following geometrical parameters: an outer radius of 20 mm, an inner radius of 8 mm, t_{AG} =1 mm, t_{PM} =1 mm, t_{Coil} =1 mm; B_r=1.35 T, N=8, P=70, Ω_R =1000 rpm, then the estimated electrical resistance of one coil is 1.2 Ω. The resistance of the single-phase (eight coils are connected into one phase) is 9.6 Ω. The constant k is determined by measuring the output voltage experimentally for the described geometry. The single-phase open circuit voltage is estimated to be V_{oc}=1.41 V. Thus, the output power of the generator can be approximated as 0.05W as calculated from equation (2). Such number can be obtained if the harvester is driven continuously at 1000 rpm. With our harvester, the speed of the generator may reach this speed, however this speed will decay exponentially as will be shown on the experimental results section. It will be shown in the experimental results that the maximum energy that can be obtained from this harvester is around 20mJ.

B) FEM Simulation

Due to the absence of high permeable magnetic bath in the construction of the harvester, the leakage and parasitic effects are high. As a consequence, the analytical calculation of the generated voltage, inductance and different design criteria affecting maximum power generation is challenging. Hence, in this section, a finite element simulation using the software Ansys Maxwell is used to calculate system inductance, and determine key design elements affecting the generated voltage and maximum efficiency point tracking, such as rotational angular velocity and air gap distance. Other design parameters, like the thickness of the coils, permanent magnet thickness, are enforced by modern production capabilities of the magnets used in the device and FR4 PCB thickness.

In order to calculate the harvester inductance, the dimension of the coil described earlier is used. For a single phase, eight coils are connected in series. The inductance of each coil is calculated using FEM simulation and compared to the measured inductance experimentally to verify the validity of the model used in the simulation. The calculated inductance is found to be 30.3 µH (or 242 µH for one phase). The measured inductance is found to be 30.75 µH (or 246 µH for one phase) which shows consistency between the experimental and simulated data. The resistance of one phase can be calculated from the dimension of the coils, with the resistance of one phase being 10.8 Ω, a value useful in the design of mf maximum efficiency point tracking. Since the measured inductance is very

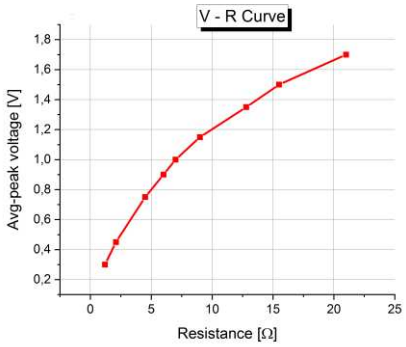

(a)

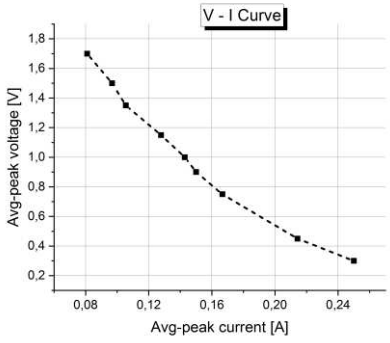

(b)

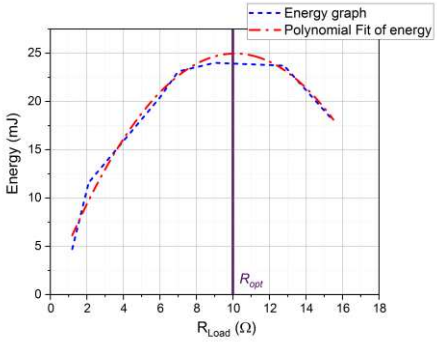

(c)

Fig.4: (a) V-R curve, (b) V-I curve, (c) output energy of an EMEH.

low, a resistive maximum efficiency point tracking system can be adopted without significant energy loss due to inductance of the coil. In addition, no phase advancing techniques are needed, even at low angular velocity (frequency).

Figure 4 (a) shows the average-to-peak terminal voltage value of the first cycle of the EMEH voltage vs. the load value connected across it. Figure 4 (b) shows the average-to-peak terminal voltage value of the first cycle of the EMEH voltage vs the average-to-peak value of the load current connected across it. Figure 4 (c) shows the variation of the generated output energy versus different loading condition. Figure 4 (c) shows that the maximum energy is achieved with a coil resistance close to 10 Ω, (R_{opt}). This value is equivalent to the total source resistance of the energy harvester. It should be noted that there is a small deviation from the resistance calculated in the analytical estimation subsection. That deviation happens as a result from the non-ideal PCB multilayer process which results in not having the exact copper thickness assumed in the analytical calculations. The graph in Fig. 4 (c) is obtained by connecting different resistances across the EMEH terminals while force is applied to the button until it compresses the spring fully (this is identical to the real application where the window presses the spring fully when it is closed). Afterwards, the button is released. The generated output voltage and current are measured with an oscilloscope. The measured current and voltage are then multiplied and the area under the curve is calculated to find the harvested energy in mJ. The mechanical system within the energy harvester has an efficiency of approximately 50%, which means the kinetic energy is roughly double the harvested energy.

The next point to be evaluated is the effect of applied velocity on the generated voltage. Knowing that the rotation of the permanent magnets are caused by free motion of the spring, the generated velocity will decay exponentially with time, causing the generator to experience a different velocity at each spring push. The effect of different applied permanent magnet velocity on the generated voltage is calculated with FEM to verify the linearity appearing in the analytical expression in equation (1). Figure 5 shows the induced voltage for different rotational speeds using the same air gap of 1 mm. The induced voltage at rotational speed of 1000 rpm reaches Vpeak- to-peak (V_{pp}) of 300mV, resulting in a total voltage per phase of 2.4V. This value decays linearly with the reduction of angular velocity.

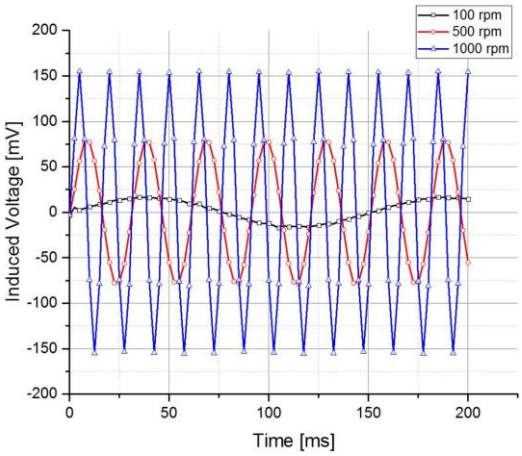

Fig. 5: Induced voltage of one coil for different rotational speed at air gap of 1mm.

The last point to be investigated is the effect of the air gap. The air gap is critical in calculating the open circuit voltage of the harvester since it is inversely proportional to the voltage. In addition, the air gap should be made large enough to reduce windage losses [38]. FEM simulation conducted shows that the magnitude of the induced voltage drops very quickly as the air gap increases. If the air gap is increased from 1 mm to 3 mm, the magnitude of the induced voltage is reduced by 50% from the initial value (i.e. the coil voltage becomes 150 mV). In order to guarantee a suitable voltage to power up the energy harvester, the air gap is selected to be 1mm.

III. Principle of Operation of the MEPT Converter

The MEPT converter, shown in Fig.6 has the same principle of operation as resistance-emulated converters used for power factor correction (PFC) applications [41]. The converter runs in discontinuous conduction mode (DCM) and hence it appears as a purely controlled resistive element to the EMEH. The input resistance of the PMS is matched with the output resistance of the EMEH and MEPT is achieved. It should be noted that the conventional solutions of using diode-based rectification cannot be used with the EMEH due to the low output voltage levels of the harvester, as mentioned earlier. As a result, the MEPT converter needs to perform ac-dc conversion in a single stage without using diode(s) connected directly to the EMEH as illustrated in the introduction section.

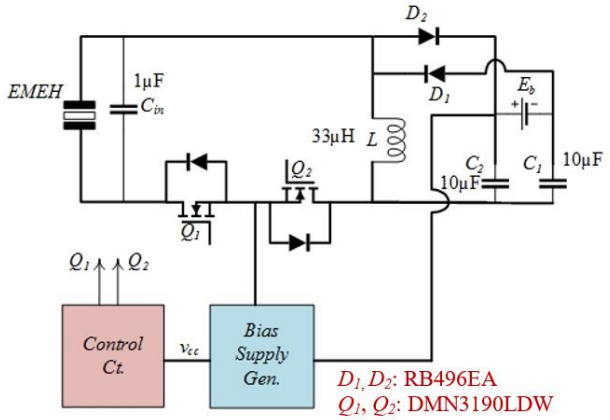

Fig.6: The presented MEPT converter.

The MEPT converter consists of two MOSFETs, two diodes, a single inductor, and two output capacitors. L, Q_1, and Q_2, are active during positive and negative half cycles of the EMEH voltage while D_1 and C_1 are active during the positive half cycle, and D_2 and C_2 are active during the negative half cycle. Q_1 and Q_2 operate simultaneously and are used for energy transfer from the EMEH to L during the first part of the switching cycle, DT_s, during both positive and negative half cycles. D_1 is used to transfer the stored energy in L to C_1 in the second part of the switching cycle, $(1\text{-}D)T_s$, during the positive

half cycle while D_2 is used to transfer the stored energy in L to C_2 during the second part of the switching cycle in the negative half cycle. Figures 7.a-d show the modes of operation of the MEPT converter during positive and negative half cycles. The input impedance of the MEPT converter is similar to the input impedance of a buck-boost converter and can be expressed as follows [13]:

$$Z_{in} = \frac{2f_S L}{D^2}, \quad (3)$$

where Z_{in} is the input impedance of the converter, L is the inductance value, f_s is the switching frequency, and D is the duty cycle. In this work, the input impedance of the converter is

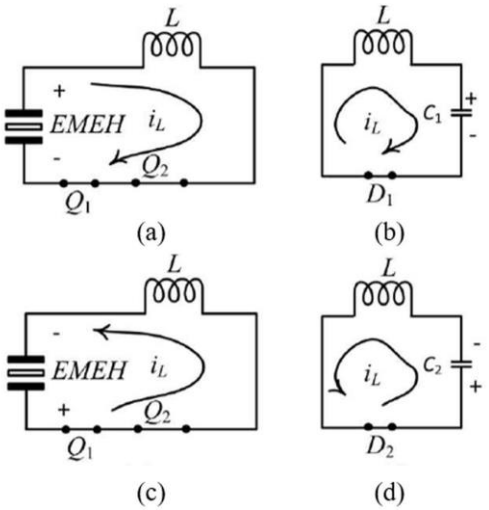

Fig.7: Modes of operation of the MEPT converter.

controlled by adjusting the duty cycle and running at a constant switching frequency. As it can be noted from Fig.6, the inductor is shared between the positive and negative half cycles, unlike many existing solutions as described thoroughly in the introduction section. Hence, size and cost improvements can be achieved, by eliminating the need for an additional inductor in the design. Another advantage of the arrangement of the topology is that Q_1 and Q_2 operate during both the positive and negative half cycles. This results in no need for synchronization with the input voltage or a zero crossing detection circuit (ZCD) [20], [35], [42]-[43], further benefitting cost, size, and losses. The advantage of two synchronous MOSFETs eliminates the need for polarity detection, a feature needed for converters that use different modes of operation during the positive and negative half cycles. The additional conduction losses of the second switch are minimized by the low voltage and current generated by the described energy harvester device. The on-state resistance of the switch is directly proportional to the blocking voltage, allowing different switches to be chosen to satisfy different application demands for efficiency. A plethora of switches exist on the market offering low on-state resistances while maintaining a form factor smaller than that of the second inductor

A) Simulation results

The principle of operation of the MEPT converter is verified using simulations as shown in Figs. 8-10. A 4V battery is used in the simulations and the EMEH is modeled as a damped sinusoidal voltage source with an output impedance of 10Ω. Figs. 8 and 9 show the operation of the MEPT converter while impedance matching takes place. Impedance matching can be further improved by filtering the EMEH current as shown in Fig. 8 (b), which is achieved by adding a small capacitor in parallel with the EMEH. Figure 9 shows the voltage across each output capacitor and the harvested current through the battery. It can be noted that the voltage across the output capacitors has the same frequency as the EMEH and the harvested current has twice the frequency, as it is being rectified. It is also worth to mention that when the capacitor voltages are equal, their ripples cancel each other out. If the capacitor voltages are unequal, the output voltage of the MEPT converter has twice the frequency of the EMEH voltage, a behavior similar to conventional PFCs. Figure 10 (a) shows the voltage across and current through both MOSFETs, Q_1 and Q_2 from Fig. 6. Figure 10 (b) shows the current through both diodes, D_1 and D_2 from Fig.7.

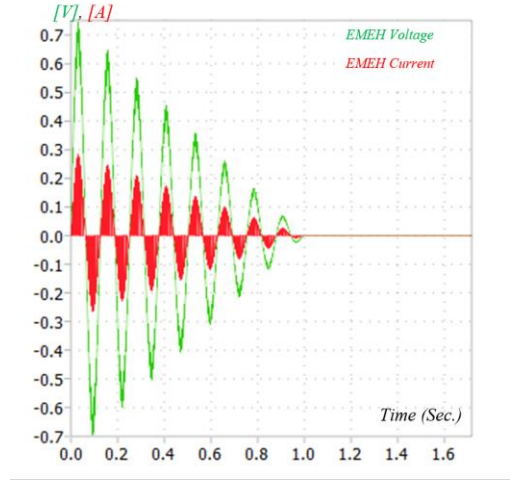

Fig.8: EMEH voltage and current with MEPT (a) without input capacitor, (b) with input capacitor.

IV. Practical Implementation

A) Bias Supply Scheme

The main idea of the bias supply scheme is to generate an

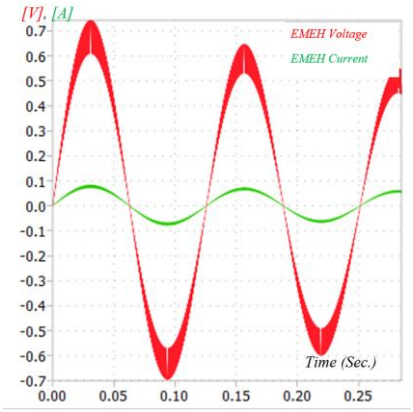

(a)

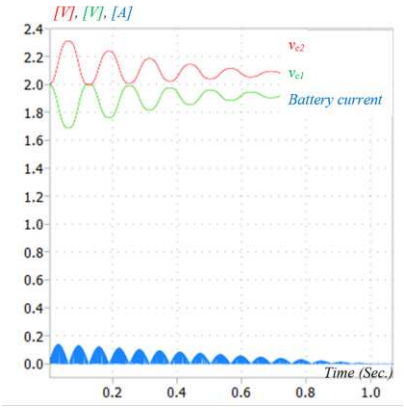

(b)

Fig.9: (a) Magnification of the EMEH voltage and current with MEPT (b) Output capacitor voltages with 4V battery and harvested current.

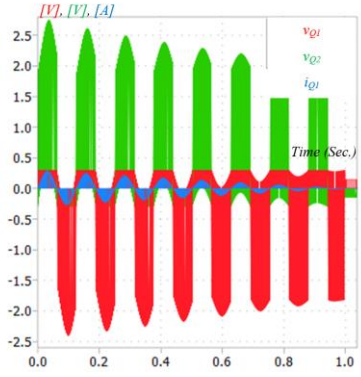

(a)

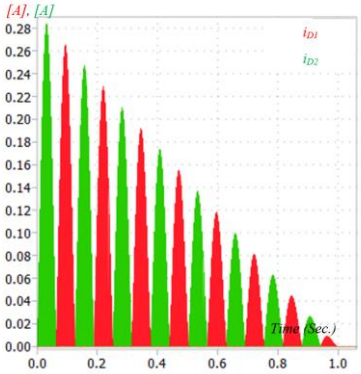

(b)

Fig.10: (a) MOSFET currents and voltages (b) Diode currents.

adequate bias supply voltage for the control circuit in two steps without the need for low threshold FETs [44]-[46], allowing the implementation of a bias supply scheme with discrete components or in a standard technology node. The first step utilizes the relatively high voltage of the very first few cycles (typically 2-3 cycles) of the damped EMEH's voltage, shown in Fig. 11, as the input of a passive a single stage Villard charge pump circuit to secure a high enough bias voltage for the control circuit, enabling the operation of the power stage. The Villard charge pump circuit consists of the two diodes D_{b1} and D_{b2} and the capacitors C_{b1} and C_{b2}. The diode, D_{b1}, is used to charge C_{b1} in the negative half cycle to the peak voltage of the EMEH, $v_{EMEH,pk}$, while D_{b2} discharges C_{b1} into C_{b2} in the positive half cycle, hence doubling the input voltage of the EMEH nominally, as shown in equation 4.

$$v_{cb2} = 2v_{EMEH,pk} - 2V_D, \quad (4)$$

where v_{cb2} is the voltage across C_{b2} and V_D is the voltage across one diode.

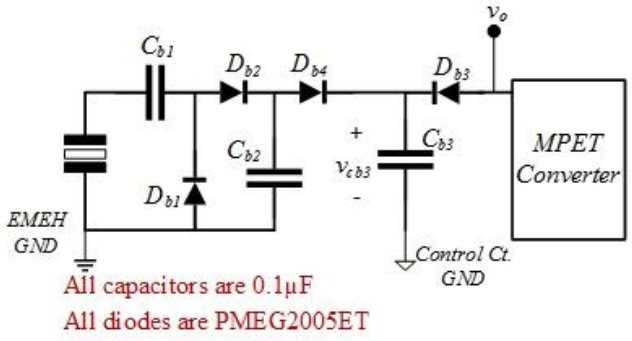

Fig. 11: First step of bias supply scheme.

The second step is based on utilizing the output voltage of the power stage highlighted in Fig.12. This provides an unregulated voltage to the downstream stage, as discussed in the next section, which acts as an input for a simple single stage charge pump circuit, formed by C_{b3} and D_{b3}, to generate a sufficient bias voltage to sustain the operation of the PMS and to make it a self-powered or standalone PMS. This simple single-stage charge pump circuit utilizes a floating capacitor whose voltage is referenced to the mid-point of the two switches of the power stage enabling the use of this capacitor as the energy source for the control circuit that controls the MOSFETs of the power stage. It is worth mentioning that the EMEHs do not require perfect impedance matching and hence fluctuations in the voltage across C_{b3} are acceptable as explained in the next subsection. Other EHs that require tight input impedance regulation can use an ultra-low power dc-dc converter to regulate the voltage across C_{b3}. Equation 5 describes the voltage across capacitor the, C_{b3} (v_{cc}), which can be found from Figs. 11&12 when D_1 conducts and C_{b3} charges.

$$v_{cc} = v_{cb3} = v_L + v_{c2} + v_{EMEH,pk} - 2V_D$$
$$= v_o + v_{EMEH,pk} - 2V_D, \quad (5)$$

where v_o is the output voltage of the MEPT converter, $v_{EMEH,pk}$ is the peak harvester voltage, and V_D is the threshold voltage of the diode. It should be noted that the ground of the bias scheme is the point of common sources of the two

MOSFETs such that the two MOSFETs can be easily driven directly by the control circuit. For proper start-up, the bleeding resistor R_b, which results in <1% losses, is connected across C_1 such that the output voltage is distributed between C_1 and C_2 to

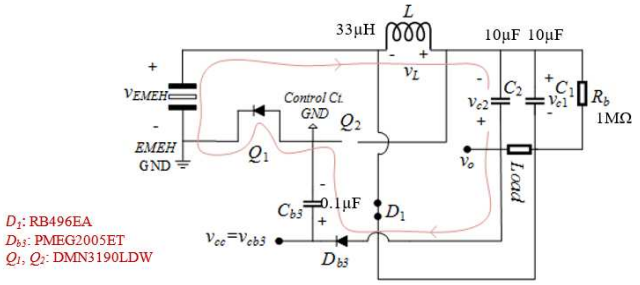

Fig. 12: Second step of the bias supply scheme.

avoid applying the full battery voltage across C_1 and hence failing of the bias scheme.

The diode, D_{b4}, is used to disconnect the Villard charge pump circuit, typically after two or three input voltage cycles typically, and allowing C_{b3} to sustain the operation of the PMS. All the diodes selected in the bias supply scheme are low-barrier Schottky diodes with a threshold voltage, V_D, of around 0.1-0.2V or less at the operating current of the circuit [47]. It should be noted that the EMEH produces power in the range of a few mW and the power consumption of the control circuit in the range of nW-µW. This implies that the power losses in the bias supply scheme can be neglected, meaning that passive simple current implementation is good for the targeted applications. For other EHs that have lower voltage than the EMEH utilized in this work and/or produce nw-µW power, a larger number of Villard charge pump stages, especially using ultra-low threshold voltage diodes [47] and/or an implementation on a standard technology node with high threshold voltage FETs that use threshold voltage cancellation techniques [44] can be used.

A difficult case for the bias supply scheme could occur if the EMEH fails to provide sufficient voltage to the charge pump circuitry. This would result in the charge pump circuitry being unable to store sufficient voltage to turn on the MOSFETs of the MEPT converter, resulting in no output at the MEPT converter. This situation is avoided by design, since the number of stages of the charge pump is defined such that the generated voltage is around 2V while the threshold voltage of the control circuit is around 0.9V [48] as shown in the next subsection. Having a factor of safety of more than two (0.9V vs 2V) provides confidence that the control circuitry will start with the targeted EMEH application as the supply.

It is worth mentioning that the power stage inductor is not only used as part of the MEPT converter but also as an essential element of the bias supply scheme as shown in Fig. 12. Unlike many existing solutions, the power stage inductor helps to boost the voltage, as shown in equation 5, and generate sufficient voltage to control the MEPT converter. The presented bias supply scheme does not requires neither dedicated control signals nor additional bulky components, helping achieve the application targets of a small solution size low extraneous power losses.

B) Control Circuit

The control circuit, shown in Fig.13, is based on two nano power comparators [48] used to from an open loop pulse width modulator (PWM) [49]. The first comparator charges C_1 through R_3 and compares the voltage to v_x such that when the voltage across C_1 is higher than v_x the comparator resets and C_1 discharges to form a triangular signal as shown in Fig. 13. The second comparator compares the triangular signal to v_y which

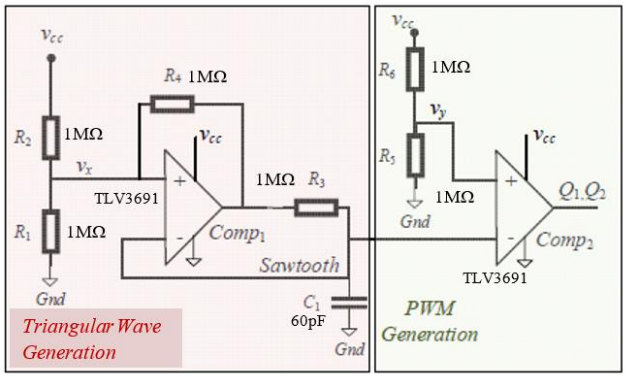

Fig. 13: Control circuit Schematic.

determines the required input impedance of the power stage and provides PWM signals to Q_1 and Q_2. Different implementations of PWM exist [50]-[52] but this approach is chosen due to the ease of implementation with discrete components and low power consumption compared to digital or op-amp based implementations. Another advantage with the full comparator technique compared with op-amp based implementations is the use of resistance values in the MΩ range, further reducing the power consumption of that block, avoiding offset, voltage-thermal noise, and parasitic impact issues. The EMEH supplies its maximum available energy at loads that are equal to Ropt±20% [10]-[11], which means it does not require a tightly regulated bias supply voltage to provide perfect resistance matching. This relaxes the requirements of the control circuit by omitting the harvester's current and voltage sensing [29]. Despite the relaxation of the regulation window, the input impedance variation remains narrow. This was validated theoretically using SPICE model simulations with a Li-Ion battery discharging from 4.2V to 2.7V yielding an impedance variation less than 3%. It is worth mentioning that the same conclusion was reached for a battery-less application where the output voltage of the MEPT converter decays as shown in the experimental results section. That happens because the control circuit operates in a weighted manner as opposed to an absolute one. This weighted operation results in a constant duty cycle throughout supply variations. This is due to the set point and average voltage value shifting in unison with supply changes. The only variations appear as minor changes in switching frequency due to amplitude variations of the triangular signal. This behavior is acceptable for the targeted energy harvesters that do not require tight impedance matching.

C) Input Capacitor

As mentioned in the previous section, an input capacitor is

used to filter the high switching frequency content of the EMEH current, as shown in Fig. 6, and hence provides a better matching and cleaner input voltage for the converter. The input capacitor is selected such that the cut off frequency, formed by the equivalent impedance of the converter and the input capacitor is lower than the switching frequency of the MEPT converter. At the same time, the input capacitor has a minimal impact on the phase shift between the EMEH current and the input current of the converter. That said, if the input capacitor is oversized, i.e a much higher capacitance value is used, a phase shift between the EMEH voltage and current takes place and affects the matching and hence the MEPT operation. If the input capacitor is extremely small in capacitance, it affects its filtering capability. An input capacitor of 1µF is used with the current implementation and results in good filtering, providing around 3Ω at the switching frequency, and does not have a negative impact on the phase as shown in the experimental results section. The aforementioned explanation can be further described by the equation describing the relationship between harvester voltage and current after adding the input capacitor, as shown in equation 6.

$$\frac{v_{EMEH}(s)}{i_{EMEH}(s)} = \frac{1}{sC_{in}+R_{opt}}, \quad (6)$$

Where $v_{EMEH}(s)$ is the harvester voltage as function of frequency, $i_{EMEH}(s)$ is the harvester current as a function of frequency, C_{in} is the input capacitor value, and R_{opt} is the optimal input impedance of the MEPT converter.

D) Highly Integrated Magnetic Based Substrate Buck Dc-Dc Converter

In order to cover batteryless applications that require tight output voltage regulation, a downstream buck stage is needed as the MEPT converter does not provide such a feature. To keep high power density of the whole PMS, conventional side-by-side assembly approaches are not favorable. It has been proven in the literature that the inductor of the buck converter is the biggest contributor to the real estate of the whole converter [53], thus the volume reduction strategy needs to be mainly directed towards the buck's inductor. The buck converter implemented in this work, switches at 4MHz, and uses a magnetic substrate. This means the substrate acts as both an inductor and a sghhnubstrate that carries the different components of the converter. This allows for the whole converter size to fit on top of the inductor resulting in a total size of 3.2mmX 2.5mm X 1.5mm. Figure 14 shows a CT scan of the magnetic based substrate where routing is implemented inside the ferrite based substrate to form the needed inductor. The ferrite-based substrate has 520nH inductance with stable characteristics up to 20MHz, a resistance of 0.5Ω at the switching frequency, rated current of 1A, and saturation current of 1.6A. Figure 15 shows the whole solution size compared to a needle head. It can be noted from Fig. 14 that the module routing is done at the corners of the substrate to reduce the parasitic inductance. In order to provide a high efficiency at light-to very light loads, the converter operates in pulse frequency modulation (PFM), or burst mode, to achieve frequency scaling depending on the load current. It is worth mentioning that the frequency scaling algorithm used in this work is the same described in [54]. Also, when the input voltage is very close to the required output voltage the converter operates as a low dropout (LDO) regulator to further improve the efficiency. In addition to that the dc-dc converter provides protection features such as short circuit, overcurrent and under voltage lockout (UVLO) protections. The magnetic substrate carries an integrated circuit, input capacitor of 2.2µF, and output capacitors, of 1µF.

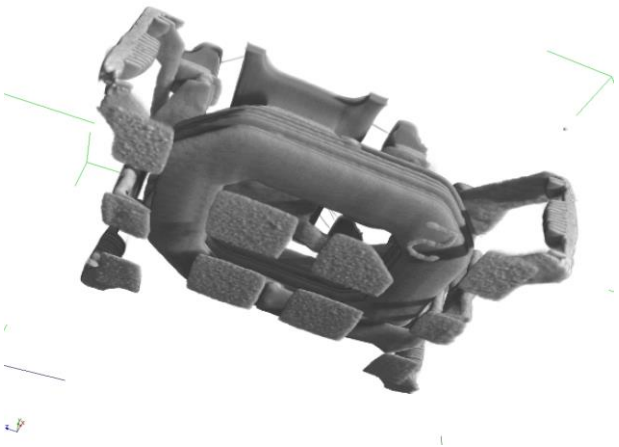

Fig. 14: CT scan of the ferrite based buck converter.

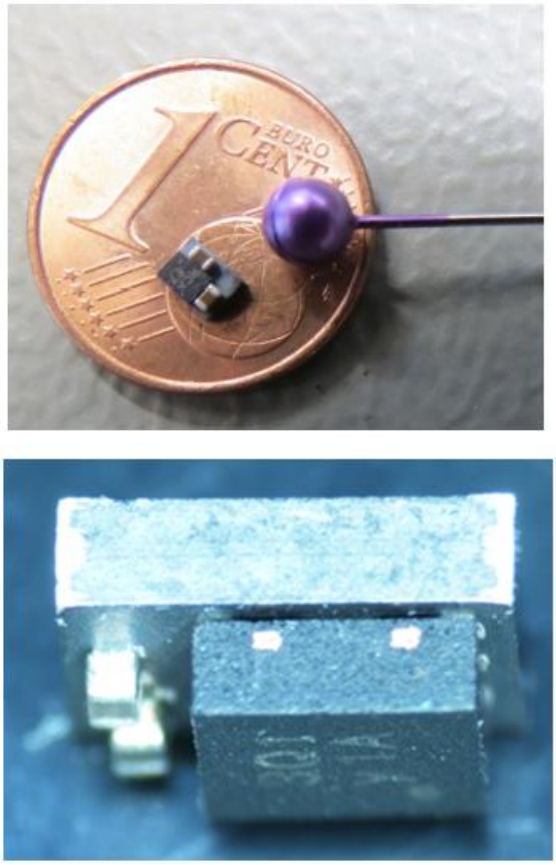

Fig. 15: The developed magnetic based substrate buck converter compaed to 1 Euro Cent and a needle head.

V. EXPERIMENTAL RESULTS

An experimental setup is built and tested to demonstrate the effectiveness of the presented approach. The optimal resistance of the EMEH is around 9.5 Ohms. Figure 16 shows the operation of the control circuit with triangular wave generation and gating pulses. Figure 17 shows MEPT capability of the

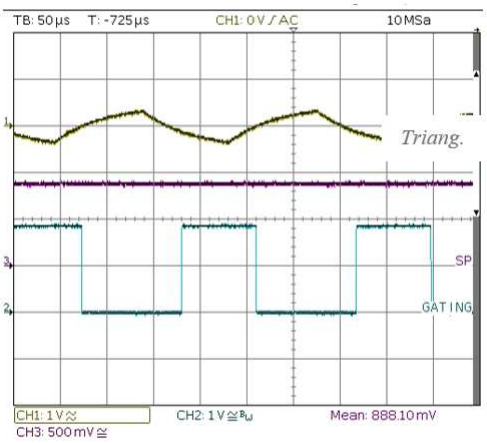

Fig. 16: Sawtooth generation and gating pulses.

PMS with a Li-Ion Battery and it can be noted that the harvester current and voltage are in phase and have a similar shape with a ratio around 9.5. Figure 18 shows the harvested current to the battery. It can be noted from Fig. 18 that a significant current is charging the battery from a single pressing of the actuator. Also, it can be noted that the battery current is the rectified version of the EMEH voltage, which demonstrates the correct operation of the MEPT converter. The PMS harvests around 17mJ, out of 20mJ (85%), when connected to 3.8V battery while the system presented in [34] harvests 12mJ and the system in [29] harvests 14mJ under the same conditions. That translates into 41.6% and

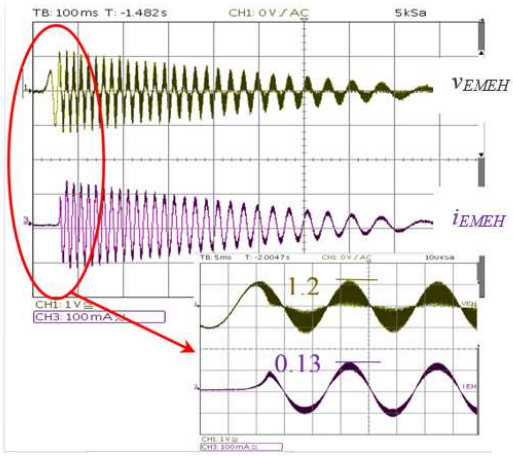

Fig. 17: Harvester's current and voltage.

21.4% more harvested energy compared to the harvested energy in [34] and [29] respectively. The improvements in the harvested energy are due to utilizing MEPT as well as running the converter in DCM, which reduces the switching losses unlike [34], and using a single inductor unlike [34] and [29].

It is worth mentioning that the efficiency of the PMS is

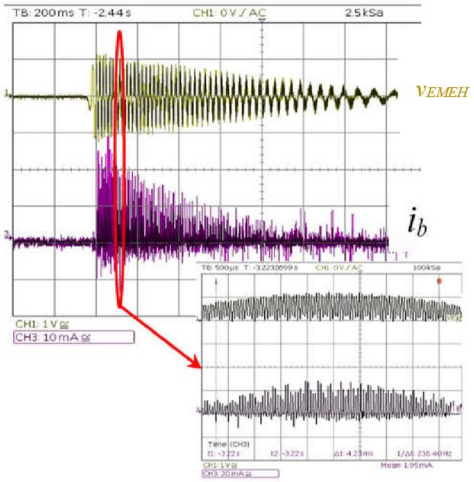

Fig.18: Harvester's voltage and the harvested current.

calculated in three steps. First, the harvester current and voltage are stored as waveforms, Fig. 17, and multiplied together in excel, and then the area under the prodcut's curve is calculated to measure the input energy to the PMS. Second, the harvested current, i_b in Fig. 18, and the battery voltage are multiplied and saved as waveforms, and then the area under the multiplications curve is calculated to measure the output energy. Finally, the efficiency of the PMS is calculated by dividing the output energy by the input energy. It should be noted that the input energy of the harvester is less than the shown values in section II (20mJ vs. 23mJ) as the experimental results show the operation of the system when integrated within a window. With the current implementation, the spring is not fully compressed and hence when it is released, it produces less energy compared to the tests performed in the lab environment shown in section II. The efficiency of the EMEH itself is around 50%, which means the input energy, generated by the pressing event, is around 40mJ. Figure 19 shows the energy flow at each section of the system for the sake of clarity.

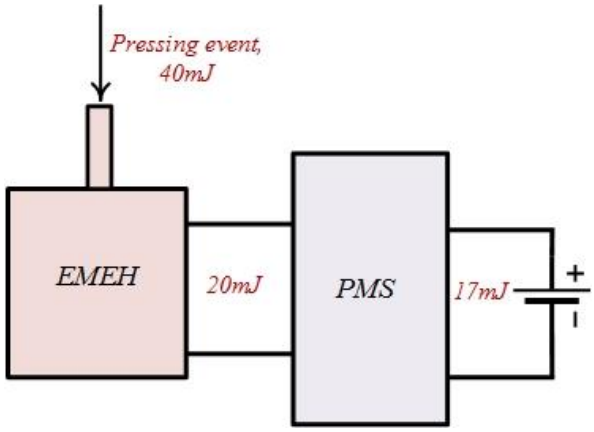

Figure 19: Energy flow in the entire system.

Figure 20 shows that input impedance variations versus cell voltage variations can be neglected, as explained in the previous section. As mentioned in the practical implementation section, the value of the bias supply voltage depends on the output stage voltage, which means that the bias supply voltage changes

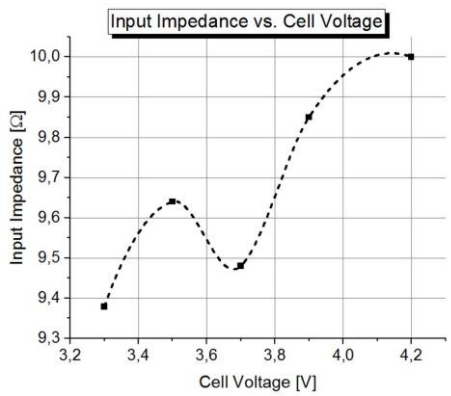

Fig. 20: Input impedance variation vs output voltage.

when the cell voltage changes. However, that change has negligible impact on the duty cycle of the converter since both the triangular waveform and the set point change by the same ratio resulting in no change in the duty cycle. On the other hand, changes in the bias supply scheme voltage result in small variations in the switching frequency of the converter, which is the main reason for input impedance variation vs. cell voltage. Figure 21 shows the MEPT converter setup and the setup presented in [34] with the same specifications. The system in [29] has the same power stage but uses two inductors. The volume of the magnetics, the largest contributor to the overall volume, in the presented MEPT converter is 32.3mm^3 while in [34] (two bulky low frequency coupled inductors) is 239.1mm^3 and in [29] is 64.6mm^3. That translates to 86.5% and 50% reductions compared to [34] and [29], respectively. It should be noted that volume reduction benefits are still valid if the MEPT converter is compared to any DCM based dual inductor solutions [28]-[31] or transformer based solutions [32]-[34]. As the volume of the used components of the entire PMS is rarely mentioned in most literature, it is a challenging task to conduct thorough bench marking of the volume of the presented solution against alternatives works in literature. That said, the authors compared the presented solution to a research-based solution that fits into DCM two inductors based solution and an industry based solution that fits into transformer based solutions since the details of both solutions can be reached relatively easy. In addition, the presented PMS has a lower BOM cost by 57.6% [29] (0.69€ vs compared to 1.65€). It is worth mentioning that the system presented in [34] is an integrated system and hence BOM comparison is not a straightforward task.

The experimental setup is also tested in batteryless applications. Figure 22 shows the bias supply voltage, v_{cb3}, and the EMEH's current, i_{EMEH}. The two steps operation of the bias supply scheme and the impedance tracking can be noticed from Fig. 22. The MEPT feature ensures that the EMEH provides its maximum allowable energy to the output of the first stage. It should be noted that the peaks of the harvester current (voltage) have the same pattern as the bias supply voltage. This in turn follows the EMEH voltage, as depicted in Eq.5. Figure 23 shows the output voltage of the first stage that provides MEPT and step-up functions, the regulated output voltage of the dc-dc buck converter, and the EMEH's current. It can be noted that the step-up stage provides as high as 6V at the output and the dc-dc converter provides a tightly regulated 1.2V at 5mA, which are the specification for wireless sensors used in IoT [55]-[57], as shown in Fig.23. Also, it can be noted that when the output voltage of the step-up stage gets lower than 2V the under voltage lockout (UVLO) in the buck converter activates as shown in Fig. 23. It is worth mentioning that the buck dc-dc converter achieves an efficiency of around 80% from load currents of 100µA up to 200mA at the given conditions, as shown in Fig. 24. It should be noted that the achieved efficiency is higher than available solutions designed for the same applications [55]. Figure 25 shows the load regulation of the buck converter. Figure 26 shows the load transient of a load step of 0mA to 5mA and back to 0mA. The frequency scaling described in [54] can be seen in Figure 26 and contributes to the flat efficiency curve shown in Fig. 24. Table 1 shows a list of the components used to develop the experimental setup. The authors also attach a video showing the operation of the harvester with a high voltage light emitting diode (LED) to demonstrate the effectiveness of the presented solutions to operate as a standalone system. For the standalone operation, none of the components used were precharged and the whole system starts with the only source being the EMEH.

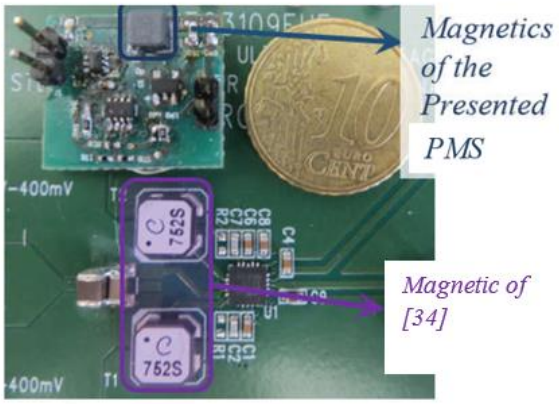

Fig.21: MEPT converter size compared to 10 Euro Cent and the solution presented in [34].

Fig. 22: Bias supply voltage and EH current.

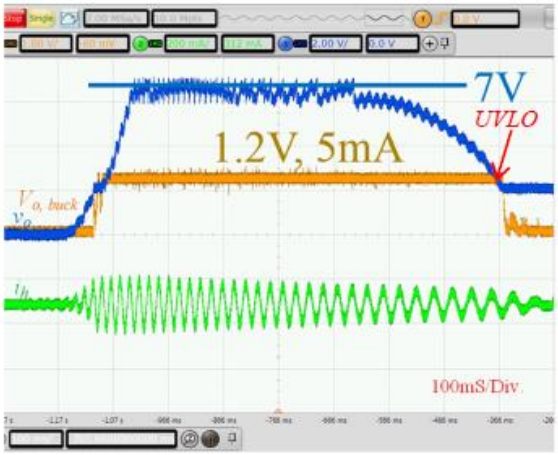

Fig.23: Output voltage of the MEPT and step-up stage, output of the buck converter, and EH current.

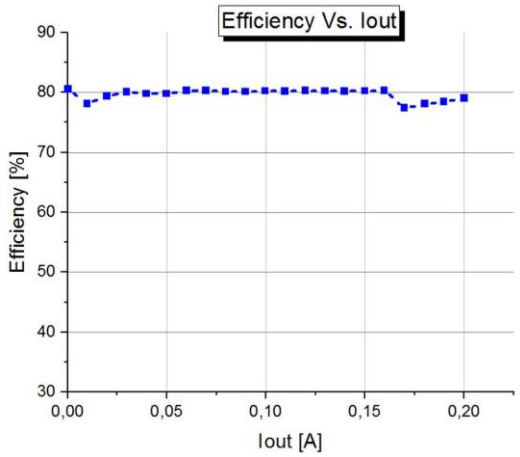

Fig. 24: Efficiency of the ferrite based substrate buck converter vs. I_{out}.

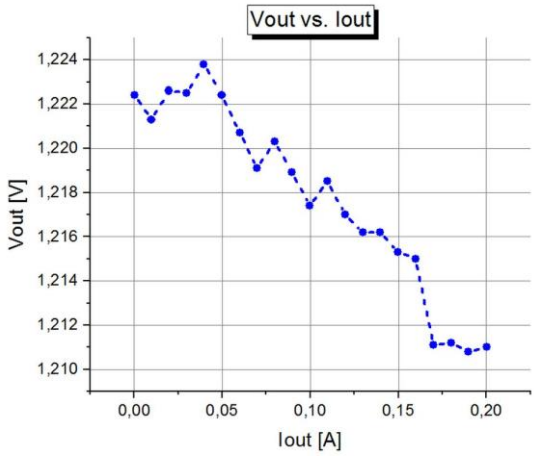

Fig. 25: Output voltage of the ferrite based substrate buck converter vs. output current.

It should be noted in real life applications, power hungry circuits are supplied by a battery, which is charged from the EMEH while the low power circuits are gathered together and supplied by the EMEH where the harvested power is sufficient to fully bias these circuits. Hence, both systems will not be powered by the same EMEH but by two EMEHs or more [8].

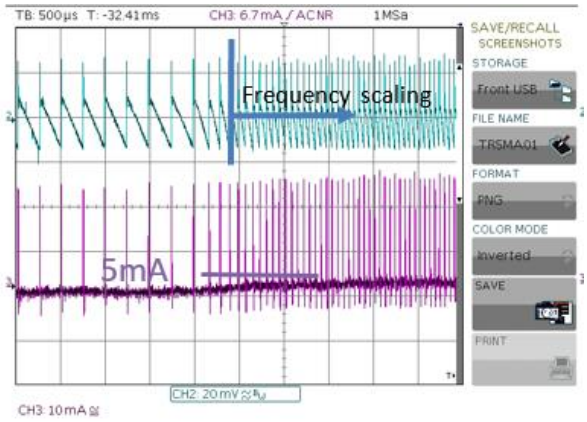

(a)

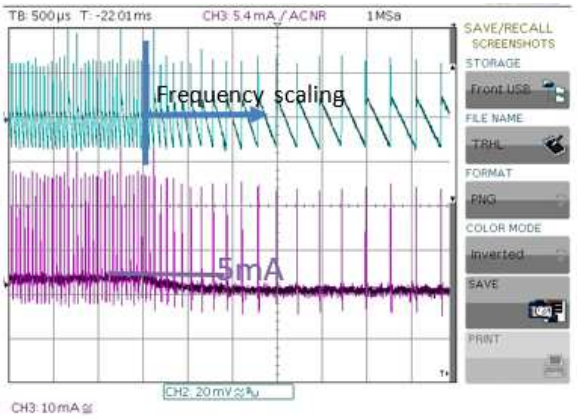

(b)

Fig. 26: Transient response of the buck converter, (a): Light-to-heavy transient. (b): Heavy-to-light transient.

TABLE I
EXPERIMENTAL STEUP PARAMETERS

Components	Parameters
MOSFETs	DMN3190LDW (Diodes Inc.)
Diodes for power stage	RB496EA (ROHM Semi.)
Diodes for bias supply scheme	PMEG2005ET (Nexperia)
Comparators	TLV3691 (Texas Instrument)
Inductor of the MEPT converter	33µH, 0.53A I_{sat} (Würth Elektronik,- 74404043330A)
Ouput capacitors of the MEPT converter	2X 10µF, 10V (Würth Elektronik,- 885012207026)
Input capacitor of the MEPT converter	1µF, 6.3V (Würth Elektronik,- 885012206002)

That is why the experimental results section did not cover having both at the same time [8].

VI. CONCLUSIONS

This paper presented a PMS for use by EMEH in battery/batteryless applications. The PMS consists of two converters, namely the MEPT converter and ferrite based substrate buck converter. The MEPT converter converts ac to

dc in a single step and provides an MEPT feature while achieving volume reduction and higher harvested energy benefits compared to many existing solutions. In addition to these advantages, the MEPT converter has a simple structure and does not require complex gate driving or control circuitry. Also, a simple, yet effective, bias supply scheme is presented in this work. The bias supply scheme enables self-powered operation and does not require pre charging prior to pressing the EMEH button as shown in the attached video, allowing for use in batteryless applications. The ferrite based buck converter shows a significant reduction in converter volume while providing high efficiency at very light load due to implementing a frequency scaling algorithm. Future work includes IC implementation of the MEPT converter and integration with passive components in a system-in-package (SiP) design [58] to provide a complete solution with only two modules, further increasing the density of the system.

ACKNOWLEDGMENT

The authors would like to thank Michael Brooks from Magi3C, Würth Elektronik eiSos for his help with English editing.

REFERENCES

[1] N.S. Shenck and J.A. Paradiso, "Energy Scavenging with Shoe-Mounted PiezoElectrics", in *IEEE Micro*, vol. 21, no. 3, pp. 3041, May/June 2001.

[2] Jingjing Zhao and Zheng You, "A Shoe-Embedded Piezoelectric Energy Harvester for Wearable Sensors," in *Sensors*, Vol. 14, no.7, pp. 12497– 12510, July 2014.

[3] Gatto and E. Frontoni, "Energy Harvesting system for smart shoes," in *Proc. 10th IEEE/ASME Int. Conf. on Mechatronic and Embedded Syst. and Applicat.*, pp. 1-6, 2014.

[4] M. A. Webb, C. Christiansen, J. Hanchett, and S. Sullivan, "Electric door release powered by an energy harvester," European patent 2378041, Jan. 4, 2017.

[5] G. Cechmanek, "Small Scale Energy Harvesting for Use with an Electronic Door Strike," MASc thesis, University of Waterloo, Ontario, 2016.

[6] T. Pennisi, "Powering IoT Applications with Energy Harvesting," Online article, *Sensors|Online*, Sep. 2016.

[7] P. Newman, "IoT Report: How Internet of Things technology is now reaching mainstream companies and consumers," Technical report, Business Insider, July 2018.

[8] *Discussions with Industry Partners*. Berlin, Germany: ELDAT, Sep. 2018.

[9] Q. Zhang, Y. Wang, and E. S. Kim, "Electromagnetic Energy Harvester With Flexible Coils and Magnetic Spring for 1–10 Hz Resonance", in *J. Microelectromech. Syst.*, vol. 24, no. 4, pp. 1193 – 1206, Aug. 2015.

[10] D. Dinulovic, M. Shousha, M. Haug, and T. Petrovic, "Portable Rotational Electromagnetic Energy Harvester for IOT," in *Proc. IEEE Int. Mag. Conf.*, pp. 1-2, 2017.

[11] D. Dinulovic, M. Shousha, M. Brooks, M. Haug, and T. Petrovic, "Push-Button Rotational Electromagnetic Energy Harvesting System," in *Proc. 61st Annu. Conf. on Magnetism and Mag. Mater.*, pp.107, 2016.

[12] P. Zeng, H. Chen, Z. Yang and A. Khaligh, "Unconventional Wearable Energy Harvesting from Human Horizontal Foot Motion," in *Proc. 36th IEEE Appl. Power Electron. Conf. Expo*., pp. 258-264, 2011.

[13] P. Zeng, and A. Khaligh, "A Permanent-Magnet Linear Motion Driven Kinetic Energy Harvester," in *IEEE Trans. Ind. Electron*., vol. 60, no. 12, pp. 5737-5746, Nov. 2012.

[14] Z. Qin, H. Talleb, S. Yan, X. Xu and Z. Ren, "Application of PGD on Parametric Modeling of a Piezoelectric Energy Harvester," in *IEEE Trans. Mag.*, vol. 52, no. 11, pp. 1-11, Nov. 2016.

[15] A. Khaligh, P. Zeng and C. Zheng, "Kinetic Energy Harvesting Using Piezoelectric and Electromagnetic Technologies—State of the Art," in *IEEE Trans. Ind. Electron.*, vol. 57, no. 3, pp. 850-860, March 2010.

[16] F. Khameneifar, S. Arzanpour and M. Moallem, "A Piezoelectric Energy Harvester for Rotary Motion Applications: Design and Experiments," in *IEEE/ASME Trans. Mechatronics*, vol. 18, no. 5, pp. 1527-1534, Oct. 2013

[17] N. Komg, D. S. Ha, A. Erturk, and D. J. Inman, "Resistive Impedance Matching Circuit for Piezoelectric Energy Harvesting," in *J. of Intell. Mater. Syst. and Structures*, Vol.21, no.13, pp. 1-10, Jan. 2010.

[18] H. Yu, J. Zhou, L. Deng, and Z. Wen, "A Vibration-Based MEMS Piezoelectric Eenergy Harvester and Power Conditioning Circuit," in *Sensors*, Vol.14, pp. 3323-3341, Feb. 2014.

[19] H. Wang, X. Shan, T. Xie and M. Fang, "Analyses of Impedance Matching for Piezoelectric Energy Harvester with a Resistive Circuit," in *proc. Int. Conf. Electron. Mech. Eng. and Informat Technol*, pp. 1679-1683, 2011.

[20] R. J. Taylor, "Optimization of a Discontinuous Conduction Mode Flyback for Acoustical Energy Harvesting," M.S. thesis, University of Florida, Gainesville, Florida, 2004.

[21] N. Kong, T. Cochran, D. S. Ha, H. C. Lin and D. J. Inman, "A Self Powered Power Management Circuit for Energy Harvested by a Piezoelectric Cantilever," in *Proc. 25th Annu. IEEE Appl. Power Electron. Conf. Expo.*, pp. 2154-2160, 2010.

[22] A. D. Brovont and S. D. Pekarek, "Modeling Air-Core PermanentMagnet Linear Generators in Free-Rotating Devices," In *Proc. IEEE Int. Electric Mach. & Drives Conf.*, pp. 735-741, 2015.

[23] S. Guo and H. Lee, "An efficiency-enhanced integrated CMOS rectifier with comparator-controlled switches for transcutaneous powered implants," in *Proc. IEEE Custom Intergrated Circuits Conf.*, 2007, pp. 385-388.

[24] G. Bawa and M. Ghovanloo, "Analysis, design, and implementation of a highefficiency full-wave rectifier in standard CMOS technology," in *IEEE J. of Analog Integrated Circuits and Signal Processing*, vol. 60, no. 1, pp. 71-81, 2009.

[25] P. M. Lin, "Topological generation and analysis of voltage multiplier circuits," in *IEEE Trans. Circuits Syst.*, vol. CAS-24, no. 10, pp. 517-530, Oct. 1977.

[26] C. K. Tse, S. C. Wong, and M. H. L. Chow, "On lossless switched capacitor power converters," in *IEEE Trans. Power Electron.*, vol. 10, no. 3, pp. 286-291, May 1995.

[27] S. Cheng, Y. Jin, Y. Rao, and D. P. Arnold, "A bridge voltage doubler ac/dc converter for low-voltage energy harvesting applications," in *Proc. PowerMEMS*, Washington D.C., Dec. 2009, pp. 25-28.

[28] S. Dwari and L. Parsa, "An efficient ac-dc step-up converter for low-voltage energy harvesting," in *IEEE Trans Power Electron.*, vol. 25, no. 8, pp. 2188-2199, Aug. 2010.

[29] M. Shousha, D. Dinulovic, and M. Haug, "A Universal Topology Based on Buck-Boost with Optimal Resistive Impedance Tracking for Energy Harvesters in Battery Powered Applications," in *Proc. 32nd Annu. IEEE Appl. Power Electron. Conf. Expo*., pp.2111-2115, 2017.

[30] P. D. Mitcheson, T. C. Green, and E. M. Yeatman, "Power processing circuits for electromagnetic, electrostatic and piezoelectric inertial energy scavengers," in *Microsyst. Technol.*, vol. 13, pp. 1629-1635, Jul. 2007.

[31] M. G. Mostafa, S. M. A. Motakabber and M. I. Ibrahimy, "Design and Analysis of a Buck-Boost Converter Circuit for Piezoelectric Energy Harvesting System," *in Proc. Int. Conf. Computer and Communication Eng.* pp. 204-207, 2016.

[32] I. D. Mayergoyz and P. McAvoy, Fundamentals of Electric Power Engineering. Singapore: World Scientific, 2014.

[33] R. Moghe, D. Divan, and F. Lambert, "Powering low-cost utility sensors using energy harvesting," in *Proc. 14th European Conf. on Power Electron. Appl.*, pp. 1-10, 2011.

[34] Linear Technology, "Auto-Polarity, Ultralow Voltage Step-Up Converter and Power Manager: LTC3109," datasheet, available: http://cds.linear.com/docs/en/datasheet/3109fb.pdf.

[35] H. Wang, Y. Tang and A. Khaligh, "A Bridgeless Boost Rectifier for Low-Voltage Energy Harvesting Applications," in *IEEE Trans. Power Electron.*, vol. 28, no. 11, pp. 5206-5214, Nov. 2013.
[36] R. Dayal, S. Dwari and L. Parsa, "Design and Implementation of a Direct AC–DC Boost Converter for Low-Voltage Energy Harvesting," in *IEEE Trans.Ind. Electron.*, vol. 58, no. 6, pp. 2387-2396, June 2011.
[37] D. Dinulovic and A. Gerfer, "Communicating Device," US Patent, US9973046B2, April 2013.
[38] S. Das, D. P. Arnold, I. Zana, J.-W. Park, M. G. Allen, and J.H. Lang, "Microfabricated High-Speed Axial-Flux Multiwatt Permanent-Magnet Generators - Part I: Modeling," in *J. Microelectromech. Syst.*, vol. 15, no. 5, pp. 1330 – 1350, Oct. 2006.
[39] D. P. Arnold, S. Das, J.-W. Park, I. Zana, J.H. Lang, M. G. Allen, "Microfabricated High-Speed Axial-Flux Multiwatt Permanent-Magnet Generators - Part II: Design, Fabrication, and Testing," in *J. Microelectromech. Syst.*, vol. 15, no. 5, pp. 1351 – 1363, Oct. 2006.
[40] C. T. Pan and T. T. Wu, "Development of a rotary electromagnetic microgenerator," in *J. Micromech. Microeng.,* vol. 17, no. 1, pp. 290 – 296, 2006.
[41] R. W. Erickson and D. Maksimovic, "Fundamentals of Power Electronics," Springer Science & Business Media, 2007.
[42] L. Mateu, L. Lühmann, H. Zessin and P. Spies, "Modified parallel SSHI AC-DC converter for piezoelectric energy harvesting power supplies," in *Proc. 33rd Annu. IEEE Int. Telecomm. Energy Conf.*, pp. 1-7, 2011.
[43] M. Eltamaly and K. E. Addoweesh, "A Novel Self-Power SSHI Circuit for Piezoelectric Energy Harvester," in *IEEE Trans. Power Electron.*, vol. 32, no. 10, pp. 7663-7673, Oct. 2017.
[44] A. A. Razavi Haeri, M. G. Karkani, M. Sharifkhani, M. Kamarei and A. Fotowat-Ahmady, "Analysis and Design of Power Harvesting Circuits for Ultra-Low Power Applications," in *IEEE Trans. Circuits Syst.*, vol. 64, no. 2, pp. 471-479, Feb. 2017.
[45] A. A. Blanco and G. A. Rincón-Mora, "A 44–93-µs 250–400-mV 0.18-µm CMOS Starter for DC-Sourced Switched-Inductor Energy Harvesters," in *IEEE Trans. Circuits Syst.*, vol. 61, no. 12, pp. 1002-1006, Dec. 2014.
[46] N. Reynders and W. Dehaene, "On the Effect of Technology Scaling on Variation-Resilient Sub-Threshold Circuits," *Solid-State Electron.*, pp.19-29, Jan. 2015.
[47] "PMEGxx05ET series, 0.5 A Very Low VF MEGA Schottky Barrier Rectifiers in SOT23 Package," *Datasheet*, Nexperia, 2010, available: https://assets.nexperia.com/documents/data-sheet/PMEGXX05ET_SER.pdf.
[48] Texas Instrument, "TLV3691 0.9V to 6.5V, Nanopower Comparator," datasheet, 2015, available: http://www.ti.com/lit/ds/symlink/tlv3691.pdf.
[49] John D. Morris and Glen Brisebois, "Rail-to-Rail Output Dual Comparator Resolves 150MHz Signals While Shifting from Analog to Digital Voltage Levels," *Linear Technology Magazine*, March 2002.
[50] J. Wittmann and B. Wicht, "A configurable based PWM generator with 2 ns on-time for >50 MHz DCDC converters," in *Proc. 11th Ph.D. Research in Microelectron. and Electron. Conf.*, pp. 41-44, 2015.
[51] J. Caldwell, "Analog Pulse Width Modulation," Texas Instrument Verified Reference Design, pp. 1-20, 2013, available: http://www.ti.com/lit/ug/slau508/slau508.pdf.
[52] Z. Lukic, N. Rahman, and A. Prodic, "Multibit Σ–Δ PWM Digital Controller IC for DC– DC Converters Operating at Switching Frequencies Beyond 10 MHz," in *IEEE Trans. Power Electron.*, Vol. 22 , no 5, 2007 pp. 1693 – 1707.
[53] M. D. Seeman, "A design methodology for switched-capacitor dc-dc converters," Ph.D. dissertation, University of California at Berkeley, 2009.
[54] W. Kim, M. S. Gupta, G. Wei and D. Brooks, "System level analysis of fast, per-core DVFS using on-chip switching regulators," in *Proc. IEEE 14th Int. Symp. High Performance Computer Architecture*, 2008, pp. 123-134.
[55] IMEC, "PMU (VIN = 1.65-3.6V, VOUT= 0-1.2V) FOR IOT AND SENSOR NODE ICs IN TSMC 40NM CMOS," datasheet, available: https://www.imec-int.com/drupal/sites/default/files/2018-11/PMU%2040nm%20Product%20Brief%20V1.0.pdf
[56] S.Yurish"IoT2.0 Sensor Innovations: Making Sense of Intelligent Sen sors," Presentation at Netware 2016, Nice, France, 24th July 2016, available:https://www.iaria.org/conferences2016/filesSENSORDEVICES16/Yurish_Tutorial_2016_Sensordevices.pdf.
[57] C. Azcona, B. Calvo, N. Medrano, S. Celma and C. Gimeno, "A 1.2-V 1.35-µW all MOS temperature sensor for wireless sensor networks," *in Proc. IEEE Int. Symp. Circuits Syst.*, pp. 365-368, 2015.
[58] S. Wolf, J. Stephan, and R. Regenhold, "ABC of Power Modules: Functionality, Structure and Hanlding of a Power Module," Swiridoff Verlag, 2015.

Mahmoud Shousha was born in Cairo, Egypt in 1986. He received the B.Sc with highest honors and M.Sc degrees from Cairo University in 2008 and 2011 respectively, and the Ph.D. degree from the University of Toronto in 2016, all in electrical engineering.
Since 2015, he has been with the Magi3C R&D department at Würth Elektronik eiSos, Munich, Germany where he develops dc-dc converter power modules. His current research interests include battery management systems, low-volume high-efficiency dc-dc converters, energy harvesting topologies, magnetics-on-silicon fabrication and characterization, and digital control of power converters.

Dragan Dinulovic (M'06) studied mechanical engineering at University of Nis (Serbia). He received his PhD from Leibniz Universität Hannover on microtechnology and MEMS in Year 2007. From 2000 to 2010 he did research at Instuute for Microtechnology (imt) in Hannover. His research area was a development of magnetic MEMS microsensors and microactuators. He was working on several EU, DFG, and BMBF projects. In 2010 he joined Würth Elektronik eiSos, where he focusses on development of thin-film inductors and transformers, on integration of passive and active power components into one package (Power supply in Package (PSiP)) or on chip (Power System on Chip (PwrSoC).

Martin Haug holds a degree in electrical and electronic engineering of the University of Applied Science in Ulm. After working more than 15 years in the area of automotive smart power ASIC design with ST Microelectronics and Bosch Semiconductor, he joined Würth Elektronik eiSos in 2014. At Würth Elektronik eiSos he is responsible for the R&D of PSiP & PwrSoC solutions.

Tomislav Petrovic obtained the B.Sc., M.Sc, and the Ph.D. degrees in 1974, 1979, and 1981 from the University of Nis, Serbia, all in mechanical engineering. He joined the Mechanical Engineering Department at the University of Nis as an Assistant Professor in 1982. In 1987 he was promoted to an Associate Professor and in 1991 he was promoted to a full Professor. His research interests include machine theory and mechanical design.

Abdelmomen Mahgoub was born in Cairo, Egypt, in 1986. He received the B.Sc. and M.Sc. degrees in electrical engineering from Cairo University, Giza, Egypt, in 2008 and 2010, respectively. He received the Ph.D. degree in electrical engineering from the interdisciplinary school for engineering science, Kyushu University, Kyushu, Japan in 2014. Between 2015 and 2016, He was a Postdoctoral Researcher in the Dipartimento di Ingegneria, Universita Degli Studi del Sannio, Benevento, Italy. Currently, he is an Assistant Professor in the Electrical Power Engineering Department, Cairo University. His current research interests include battery management and chargers' systems, low-volume high-efficiency dc-dc converters, resonant converters, multilevel inverters, and energy harvesting technologies.